

## ARE 2I/BORISOV AND OORT CLOUD COMETS ALIKE?

ZDENEK SEKANINA

Jet Propulsion Laboratory, California Institute of Technology, 4800 Oak Grove Drive, Pasadena, CA 91109, U.S.A.  
*Version March 13, 2024*

### ABSTRACT

The interstellar comet 2I/Borisov bears a strong resemblance to Oort Cloud comets, judging from its appearance in images taken over the first six weeks of observation. To test the proposed affinity in more diagnostic terms, 2I is compared to Oort Cloud comets of similar perihelion distance, near 2 AU. Eight such objects are identified among the cataloged comets whose orbits have been determined with high accuracy. This work focuses on three particular characteristics: the light curve, the geometry of the dust tail, and the dust parameter  $Afp$ . Unlike Oort Cloud comets with perihelia beyond the snow line, Oort Cloud comets with perihelia near 2 AU show strong evidence of the original halo of slowly accelerating, millimeter-sized and larger icy-dust grains only in early tail observations. The dust tail in later images is primarily the product of subsequent, water-sublimation driven activity nearer perihelion but not of activity just preceding observation, which suggests the absence of microscopic-dust ejecta. Comet 2I fits, in broad terms, the properties of the Oort Cloud comets with perihelia near 2 AU and of fairly low activity. Future tests of the preliminary conclusions are proposed.

*Subject headings:* comets: individual (2I/Borisov, Oort Cloud comets) — methods: data analysis

### 1. INTRODUCTION

The era of interstellar comets is upon us, having had so far the flavor of a bizarre story. Less than two years after the hectic weeks with a weird cometary cocoon designated 1I/‘Oumuamua, whose nature is still shrouded in mystery, Gennady Borisov, a Russian *amateur* astronomer, has pulled the proverbial rabbit out of a hat by discovering, on 2019 August 30, the *first active interstellar comet*, of apparent magnitude 18, with a *65-cm telescope* (!) of his own design (Green 2019, O’Callaghan 2019). Borisov’s find is a stunning achievement by any measure, especially in the light of the post-‘Oumuamua nearly universal consensus that instrumentation more powerful than currently available is needed to successfully search for further interstellar objects. While this perception is prudent in follow-up studies, Borisov’s discovery demonstrates that ever bigger telescopes are by no means indispensable in meeting the basic objective.

While the comet’s interstellar origin had been flagged by a hyperbolic-motion search code on September 8 (Guzik et al. 2019), the official designation 2I/Borisov was inexplicably delayed until September 24, or 25 days after discovery. To assign the designation 1I to ‘Oumuamua took only 19 days, even though groundbreaking and time-consuming IAU negotiations were then involved.

The new comet is bound to trigger revised estimates of the population of interstellar comets. On the one hand, one should be wary of the law of small numbers, on the other hand it is true that discoveries of comets of apparent magnitude around 18 have been fairly common for close to 70 years, essentially since the time the 122-cm Schmidt telescope became operational at Palomar in late 1948 (e.g., Harrington 1952). Records show that comet C/1954 M1 was at the time of discovery of magnitude 19 (e.g., Porter 1955). It thus took at least 65 years to discover the first interstellar comet as faint as 2I/Borisov at a fairly large geocentric distance.

### 2. THE ORBIT ECCENTRICITY

Although the orbit eccentricity of 2I/Borisov is much higher than that of 1I/‘Oumuamua, both values are approximately what one expects, if either object arrived from a star system whose velocity relative to the Sun is near a statistically averaged value determined by modeling the kinematics of main-sequence stars and the Sun’s motion with respect to the Local Standard of Rest (LSR). For the averaged velocity  $V_{\text{rel}}$  of an interstellar object upon its approach to the Sun one finds

$$\langle V_{\text{rel}}^2 \rangle = V_{\text{sun}}^2 + \langle \sigma_V^2 \rangle, \quad (1)$$

where  $V_{\text{sun}}$  is the Sun’s velocity with respect to the LSR and  $\sigma_V$  is the mean dispersion of star velocities, which according to Dehnen & Binney (1998) is a function of the  $B-V$  color, increasing from blue to red stars. These authors find a color independent  $V_{\text{sun}} = 13.4 \text{ km s}^{-1}$  and from their results it follows that  $\langle \sigma_V^2 \rangle^{\frac{1}{2}} = 28.3 \text{ km s}^{-1}$  for stars in the  $B-V$  range of +0.14 to +0.47 mag. Equation (1) yields  $\langle V_{\text{rel}}^2 \rangle^{\frac{1}{2}} = 31.3 \text{ km s}^{-1}$  and the eccentricity  $e$  is related to the perihelion distance  $q$  (in units of AU) by

$$e = 1 + \frac{\langle V_{\text{rel}}^2 \rangle}{V_{\text{earth}}^2} q, \quad (2)$$

where  $V_{\text{earth}} = 29.78 \text{ km s}^{-1}$  is the Earth’s mean orbital velocity. For ‘Oumuamua  $q = 0.255 \text{ AU}$  and the predicted  $e = 1.28$  is close to the actual value of 1.20; for Borisov’s comet  $q = 2.01 \text{ AU}$  and the predicted  $e = 3.22$  is not too far from the actual value of 3.36.<sup>1</sup>

On the other hand, the eccentricity effect on orbital velocities of the two objects turns out to be dramatic. At the perihelion and discovery times the parabolic limits were exceeded, respectively, by 8 percent and 21 percent for 1I/‘Oumuamua, but by 48 percent and 66 percent in the case of 2I/Borisov.

Electronic address: Zdenek.Sekanina@jpl.nasa.gov.

<sup>1</sup> Comparison made with the elements in MPEC 2019-T116.

**Table 1**  
Oort Cloud Comets As Potential Analogs for 2I/Borisov

| Comet                              | Perihelion distance $q$ (AU) | Original barycentric reciprocal semimajor axis $(1/a_b)_{\text{orig}}$ (AU $^{-1}$ ) | Perihelion time (TT) | First obs. used <sup>a</sup> | Covered orbital arc (days) | Number of obs. used | Orbit quality code |
|------------------------------------|------------------------------|--|----------------------|------------------------------|----------------------------|---------------------|--------------------|
| C/2011 L2 (McNaught)               | 1.938                        | $-0.000\,024\,2 \pm 0.000\,004\,7^b$   | 2011 Nov 01.27       | −152                         | 240                        | 52                  | 1A                 |
| C/2018 C2 (Lemmon)                 | 1.957                        | $+0.000\,037\,0 \pm 0.000\,000\,7^c$   | 2018 Jun 02.22       | −125                         | 272                        | 1645                | 1A                 |
| C/2006 L2 (McNaught)               | 1.994                        | $+0.000\,009\,8 \pm 0.000\,001\,7^d$   | 2006 Nov 20.20       | −159                         | 388                        | 380                 | 1A                 |
| C/2014 AA <sub>52</sub> (Catalina) | 2.003                        | $+0.000\,029\,4 \pm 0.000\,000\,9^e$   | 2015 Feb 27.65       | −419                         | 624                        | 365                 | 1A                 |
| C/2008 J6 (Hill)                   | 2.004                        | $-0.000\,025\,3 \pm 0.000\,002\,3^f$   | 2008 Apr 10.94       | −230                         | 471                        | 337                 | 1A                 |
| C/1907 E1 (Giacobini)              | 2.052                        | $+0.000\,025\,1 \pm 0.000\,019^g$  | 1907 Mar 19.61       | −10                          | 354                        | 67                  | 1B                 |
| C/2011 R1 (McNaught)               | 2.080                        | $+0.000\,031\,1 \pm 0.000\,000\,3^h$   | 2012 Oct 19.62       | −739                         | 1246                       | 1304                | 1A                 |
| C/1948 E1 (Pajdušáková-Mrkos)      | 2.107                        | $+0.000\,033\,7 \pm 0.000\,004^i$  | 1948 May 16.61       | −64                          | 698                        | 95                  | 1A                 |

**Notes.**

<sup>a</sup> Time reckoned in days from perihelion: negative means before perihelion; may include pre-discovery observations.

<sup>b</sup> Nakano (NK 2197) lists  $-0.000\,046 \pm 0.000\,008\,6$  AU $^{-1}$ .

<sup>c</sup> Nakano (NK 3761) lists  $+0.000\,028 \pm 0.000\,000\,7$  AU $^{-1}$ .

<sup>d</sup> Królikowska & Dybczyński (2013) list  $+0.000\,012\,9 \pm 0.000\,001\,4$  AU $^{-1}$ , while Nakano (NK 1713) finds  $0.000\,000 \pm 0.000\,001\,6$  AU $^{-1}$ .

<sup>e</sup> Nakano (NK 3124) lists  $+0.000\,016 \pm 0.000\,001\,0$  AU $^{-1}$ .

<sup>f</sup> Nakano (NK 2397) lists  $-0.000\,019 \pm 0.000\,003\,9$  AU $^{-1}$ , while Królikowska & Dybczyński (2013) from only post-perihelion observations find  $+0.000\,025\,4 \pm 0.000\,004\,0$  AU $^{-1}$ .

<sup>g</sup> Królikowska et al. (2014) list  $+0.000\,033\,8 \pm 0.000\,021\,6$  AU $^{-1}$ .

<sup>h</sup> Nakano (NK 2647) lists  $+0.000\,020 \pm 0.000\,000\,4$  AU $^{-1}$ .

<sup>i</sup> Królikowska et al. (2013) list  $+0.000\,037\,3 \pm 0.000\,002\,7$  AU $^{-1}$ .

### 3. 1I/‘OUMUAMUA CONTRA 2I/BORISOV: TRAITS SHARED WITH OORT CLOUD COMETS

Investigations of the physical and compositional properties of 2I/Borisov have already begun (e.g., Guzik et al. 2019; Fitzsimmons et al. 2019; Yang et al. 2019; de León et al. 2019; Dybczyński et al. 2019; Jewitt & Luu 2019; Karetta et al. 2019) and will surely continue. cursory inspection of the appearance of the comet suggests its *striking similarity to Oort Cloud comets*, unlike 1I/‘Oumuamua, which has often been described as an object unlike any other ever observed. Yet, ‘Oumuamua could be a piece of debris of a dwarf interstellar comet, which, because of its small perihelion distance, had disintegrated near perihelion (Sekanina 2019a). Intrinsically faint, dust-poor Oort Cloud comets with perihelia closer to the Sun than  $\sim 0.5$  AU are known to do just that (Sekanina 2019b). In the process of disintegration, the properties of the parent body altered to the extent that ‘Oumuamua as a fragment could not be expected to provide information on the body that had arrived from interstellar space. 2I/Borisov is expected to be largely immune to such a mishap because of its distant orbit.

Most members of the Oort Cloud population have their perihelion distances beyond the snow line and their impressive preperihelion activity at large heliocentric distances is being driven by processes other than the sublimation of water ice. Referring to three such objects — C/1954 O2 (Baade), C/1954 Y1 (Haro-Chavira), and C/1956 F1 (Wirtanen) — Roemer (1962) described their appearance by remarking that a featureless, rectilinear tail emanates from a clearly bounded envelope around the nuclear condensation. The tail is very nearly parallel-sided, its width essentially unchanged and equal to the diameter of the head up to the point of extremity. This applies equally after perihelion, when dust tails of other comets have a tendency to broaden considerably.

Osterbrock (1958) noted that the tails of comets Baade and Haro-Chavira were oriented about midway between the antisolar direction and the orbit behind the nucleus. This puzzle was eventually settled by Sekanina’s (1973, 1975) proposal of the conservation-of-momentum law’s effect on *sizable dust grains* released at *very low velocities* from the nucleus *far from the Sun* (up to 10 AU or more) on the way to perihelion. The problem of activity of Oort Cloud (and some other) distant comets long before perihelion was recently revisited by Meech et al. (2009).

If active interstellar comets, such as 2I/Borisov, and Oort Cloud comets are alike, their similarity should extend far beyond their mere appearance. If so, it is essential that the dependence of cometary activity on heliocentric distance be recognized in undertaken tests of diagnostic physical signatures. Accordingly, the behavior of 2I/Borisov should be compared with Oort Cloud comets of similar perihelion distance.

### 4. POTENTIAL ANALOGS TO 2I/BORISOV

Since the orbital computations showed that the perihelion distance of 2I/Borisov equals almost exactly 2.0 AU, I searched for cataloged long-period comets whose orbits match this condition to within  $\pm 0.1$  AU. I found a total of 26 objects since 1890, of which nine were observed poorly enough that only a parabolic orbit could be computed. Of the 17 remaining entries only eight were *bona fide* Oort Cloud comets, with an original barycentric reciprocal semimajor axis,  $(1/a_b)_{\text{orig}}$ , not exceeding  $+0.000\,050$  AU $^{-1}$ , i.e., with the aphelion distance not below 40 000 AU; they are listed in Table 1 in the order of increasing perihelion distance.<sup>2</sup> The values of  $(1/a_b)_{\text{orig}}$

<sup>2</sup> Two comets, C/1890 F1 (Brooks) and C/1993 A1 (Mueller), have  $(1/a_b)_{\text{orig}}$  that is larger than  $+0.000\,050$  AU $^{-1}$  but smaller than  $+0.000\,100$  AU $^{-1}$ , i.e., aphelia between 20 000 and 40 000 AU.

are taken from the website of the *Minor Planet Center*<sup>3</sup> (MPC), but independent values from two other sources, the Warsaw group and S. Nakano, are presented in the footnotes to Table 1. The orbit quality in the last column is described by the classification scale introduced by Marsden et al. (1978). An important point is that none of the tabulated comets required inclusion of non-gravitational terms into the equations of orbital motion. However, it is noted that for two of the eight comets  $(1/a_b)_{\text{orig}} < 0$ , a potential signature of small nongravitational effects that have been unaccounted for (Marsden et al. 1978).

The case of C/2008 J6 is particularly suspicious because Królikowska & Dybczyński (2013) — unlike either the MPC or Nakano — obtained a positive value of  $(1/a_b)_{\text{orig}}$  by skipping the pre-discovery single-night observations made by the Siding Spring Survey more than seven months before perihelion (see below). On the other hand, they attempted a nongravitational orbital solution for comet C/2006 L2 and did not find it at all helpful. The Oort Cloud analogs thus suggest that a measurable *nongravitational acceleration in the orbital motion of 2I/Borisov should not be ruled out* altogether, yet its detection may be difficult and the magnitude certainly much lower than for 1I/‘Oumuamua.

In the following, information is presented for each of the eight Oort Cloud analogs of 2I/Borisov, arranged chronologically.

#### *Comet C/1907 E1 (Giacobini)*<sup>4</sup>

Discovered on 1907 March 9 (Bassot 1907), only one week before perihelion, this comet was poorly observed for brightness, in part because it was moving toward the Sun in the sky and became lost in twilight. The peak apparent magnitude of 11 was consistently reported by at least four independent observers within 72 hours of the discovery, but it is not possible to assess the degree to which do these estimates represent the comet’s total brightness.

Using the ephemeris by Weiss (1907a, 1907b), Wolf (1907) recovered the comet on December 4. Much fainter than at the time of discovery, it was then observed until 1908 February 26, which allowed the computation of an orbit of high enough quality to recognize the object as a member of the Oort Cloud (Marsden et al. 1978).

#### *Comet C/1948 E1 (Pajdušáková-Mrkos)*<sup>5</sup>

The discovery of this 10th magnitude object was made first by L. Pajdušáková and then, dispelling her subsequent doubts about the find by getting a photographic image, A. Mrkos on 1948 March 13 (Merton 1949), more than nine weeks before perihelion. Van Biesbroeck (1950) later detected the comet’s images on photographic plates taken on February 15 and March 5, extending the preperihelion orbital arc covered by observations to 91 days.

A systematic series of 132 visual-brightness estimates was secured by Beyer (1950), who also provided data sets on the orientation and length of the comet’s dust tail (Section 6). Comparison shows that the magnitudes by

Beyer and Van Biesbroeck were entirely compatible, so that the February 15 pre-discovery data point can readily be linked with the rest of the observations.

#### *Comet C/2006 L2 (McNaught)*

A product of the Siding Spring Survey, this comet was discovered by McNaught (2006) on 2006 June 14, more than five months before perihelion when it was of magnitude 13.7. An extensive set of CCD photometric observations, reported as total magnitudes, was provided by K. Kadota (observatory code 349; footnote 3) between August 2006 and April 2007.

#### *Comet C/2008 J6 (Hill)*

This object was not discovered until five weeks after perihelion (Hill 2008), when it was of magnitude 15.5 and had a clear nuclear condensation. The only preperihelion observations are CCD images found years later on four exposures taken nearly nine months before discovery on a single night by McNaught (2013). Because of the post-perihelion discovery, information on this comet is not used in the following.

#### *Comet C/2011 L2 (McNaught)*

Another catch by McNaught (2011a), of magnitude 18.1, was secured on 2011 June 2, about five months before perihelion. The comet was observed over a period of less than three months, followed by a five-months gap of no reported observation. The object was then at high southern declinations, yet staying more than 50° from the Sun. Resuming only in mid-January 2012, the observations terminated before the end of that month. Because of the gap, the comet is not explored below.

#### *Comet C/2011 R1 (McNaught)*

Discovered on 2011 September 3, more than a year before perihelion, with a strongly condensed coma and of magnitude 16.5 (McNaught 2011b), this comet was later detected on 12 exposures obtained at the Catalina Sky Survey on 2010 October 10 and November 6 and 30 (Hill et al. 2012) and on three exposures taken at the ISON-NM Observatory, Mayhill, also on October 10 (Elenin 2012), thus extending the preperihelion orbital arc under observation to slightly more than two years. Since the comet was last detected in mid-April 2014, the observations cover nearly 3.5 years, clearly the record among the objects in Table 1. Images from 2013 show a long, narrow tail, as the Earth was approaching its transit across the comet’s orbital plane.

#### *Comet C/2014 AA<sub>52</sub> (Catalina)*

When discovered by Kowalski (2014) in Catalina Sky Survey images from 2014 January 11, about seven weeks before perihelion, this object — slightly brighter than magnitude 20 — had a stellar appearance and was classified as an asteroid. However, when imaged near perihelion, on February 24, by Bolin et al. (2014) of the Pan-STARRS Project at Haleakala, the object had a strongly asymmetric appearance (also confirmed at Siding Spring) and was reclassified as a comet (Williams 2014). This report also listed two pre-discovery astrometric observa-

<sup>3</sup> See [https://minorplanetcenter.net/db\\_search](https://minorplanetcenter.net/db_search).

<sup>4</sup> Old designation 1907a = 1907 I.

<sup>5</sup> Old designation 1948d = 1948 V.

tions from Haleakala. A slender tail is prominently seen in images taken months before perihelion.

Even though the comet was under observation over 21 months, until late-September of 2015, there were two major gaps: the first extended from late May to late September 2014, the second from late February to late July 2015; both were centered on times of small solar elongations.

#### *Comet C/2018 C2 (Lemmon)*

An apparently asteroidal object of magnitude 20, discovered by the Mount Lemmon Survey (2018) on 2018 February 5, four months before perihelion, was found to be marginally extended with a faint tail in CCD images taken at Mauna Kea on March 22 (Micheli 2018). Additional Lemmon images were soon found from January 28 (Gibbs et al. 2018).

This appears to be the intrinsically faintest of the eight comets in Table 1. The observations terminated while the object was still at least three magnitudes brighter than at discovery, but its solar elongation was dropping rapidly into twilight.

Since no data on the chemical composition appear to exist on these comets that could be used diagnostically to examine the degree of correspondence in the behavior of 2I/Borisov and the Oort Cloud comets, I focus in the following on three fundamental physical characteristics, namely:

- (1) the overall light curve, including the dependence of the preperihelion intrinsic brightness on heliocentric distance, and potential short-term variations;
- (2) imaging of a narrow, featureless dust tail, its orientation and projected length as a function of time; and
- (3) the  $Afp$  parameter, a dust production proxy introduced by A’Hearn et al. (1984), as a function of heliocentric distance along the preperihelion arc of the orbit.

#### 5. THE LIGHT CURVES

A temporal variation of a comet’s total brightness normalized to a unit distance from the Earth provides important information on the object’s activity. It not only describes the systematic rate of brightening before perihelion and fading after perihelion, but also shows the position of the brightness peak relative to perihelion and discloses instances of flare-ups, whether sudden outbursts or more gradual surges as well as of unexpected dips in brightness. The rate of variation with heliocentric distance  $r$  is diagnostic of the comet’s physical state; for example, an  $r^{-2}$  trend for a dust-rich comet is characteristic of a constant cross-sectional area of grains in the atmosphere.

The enormous temporal span of the comets in Table 1, more than a century, entails a problem for maintaining uniformity in the presentation of the light curves because of the light-detector evolution over this period of time. Chronologically, the first two comets — C/1907 E1 and C/1948 E1 — come from the era of visual and photographic observations, while the remaining comets from the era of CCD observations, even though traditional inspection of comets by visual methods has continued to the present time.

To meaningfully relate the light curves derived by different techniques, it is essential to establish standards allowing comparison of photometric systems of individual observers. There are at least three issues involved: (i) the relationship between the total magnitudes derived visually and from CCD images; (ii) the major difference between the photometric behavior of the nuclear condensation and the comet as a whole; and (iii) the usage of a variety of scanning apertures and color filters in CCD imaging. An additional problem is that of correcting for a phase effect, which is being taken care of in this paper by applying the Marcus (2007) standard law for dust-rich comets. Phase angles are limited to  $< 30^\circ$ .

As far as I know, only CCD magnitudes have so far been reported for 2I/Borisov. Accordingly, I collected this type of photometric data for the selected Oort Cloud analogs as well. As described in some detail elsewhere (Sekanina 2017), complications could be mitigated by restricting the CCD data set to total magnitudes only and by introducing a system of appropriate corrections for individual observers to convert their data to a common photometric scale. Ultimately, the scaled total CCD magnitudes of the analog comets have been converted to total visual magnitudes (normally obtained by estimating bright comets with the naked eye, binoculars, or other small instruments), using comparisons of a few overlapping data obtained by either method for C/2011 R1 when it was at its brightest. These have shown that — to the extent allowed by the uncertainties involved — the total brightness is visually about 1.5 mag higher than the total CCD magnitudes indicate.

Given that light curves with the preperihelion branch missing or with gaps extending over long periods of time are deemed unsuitable for this type of investigation, only four comets from Table 1 have qualified as potential 2I light-curve analogs of interest — C/1948 E1, C/2006 L2, C/2011 R1, and C/2018 C2. The light curves, in which the estimated total visual brightness is represented by the magnitude  $H_\Delta$ , normalized to a geocentric distance of 1 AU and to a zero phase angle, are plotted in Figure 1. They provide information on the nature of these objects to be confronted with the light curve of 2I/Borisov when available. First, the scaling errors notwithstanding, enormous differences clearly exist in the degree of activity among the four comets, equivalent at perihelion to a factor of  $\sim 300$  in brightness. Second, the two comets for which the data are about evenly distributed before and after perihelion — C/2006 L2 and especially C/2011 R1 — suggest that the post-perihelion branch of the light curve is steeper, a well-known property of Oort Cloud comets (e.g., Whipple 1978). An inflection or a possible minor dip before perihelion are apparent on either of them. The pre-discovery observations of C/2011 R1, made about two years prior to perihelion, are well outside the boundary of the plot in Figure 1, but they closely conform to the light-curve fit. Evidence for C/2018 C2 is inconclusive because the post-perihelion branch of its light curve is cut short by the comet’s disappearance in twilight, while C/1948 E1 appears to have experienced a brightness surge (but not an outburst) in the weeks just before perihelion. And third, with the exception of C/1948 E1, whose light curve near its maximum is distorted by the surge, the comets achieve peak brightness some 6–7 weeks after perihelion.

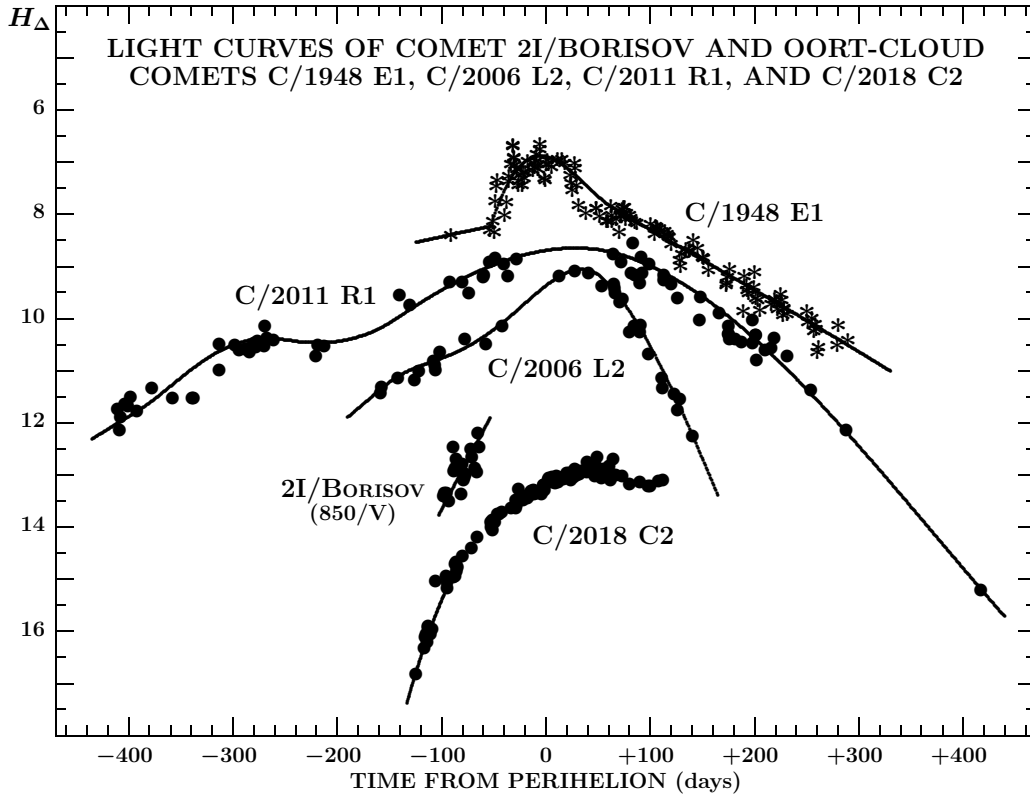


**Figure 1.** Light curves of four Oort Cloud comets with perihelia near 2 AU and a version of 2I/Borisov's light curve. For C/2006 L2 and C/2011 R1, the total CCD magnitudes normalized to a unit geocentric distance, corrected for the phase effect using the Marcus (2007) standard law for dust-rich comets, and converted approximately to the visual photometric scale,  $H_{\Delta}$ , are plotted against time, reckoned from perihelion time. For C/2018 C2 there was no difference between total and nuclear CCD magnitudes. For C/1948 E1 the plotted data are Beyer's (1950) uncorrected visual magnitudes. Different symbols used for C/1948 E1 prevent confusion with the overlapping data for C/2011 R1. The pre-discovery observations of C/2011 R1 are way outside the plot, but fit the light curve. The only points plotted for 2I/Borisov are the corrected data from code 850 (with use of a V filter), but because of the comet's excessively high orbital velocity, the relation between the brightness and time does not properly reflect the position of the interstellar comet relative to the Oort Cloud analogs; a plot against heliocentric distance in Figure 2 is more representative.

For 2I/Borisov, the set of plotted data presents daily averages of the code 850 magnitudes, obtained with a V filter and reported on the Minor Planet Electronic Circulars (MPEC). As of early October, this has been the most extensive set of data available from a single observing site (20 points). Each is the mean of several, usually three, individually reported entries, some of which turned out to be remarkably consistent with one another, whereas others showed fairly large scatter. After some experimentation, the factor used to convert the averaged magnitudes to the adopted standard system of total visual magnitudes was found to be about  $-2.1$  mag. cursory inspection shows that compared to the light curves of the Oort Cloud analogs the data are surprisingly noisy. The location of 2I in the plot is closer to the lower end of the intrinsic-brightness range, but this may not necessarily be the case. Two important points are in order: (i) the CCD magnitude determinations vary from observer to observer, so the data presented here are largely unsupported; and (ii) the plot of intrinsic brightness against time does not do the comparison with the Oort Cloud comets justice because of 2I's much higher orbital speed.

To remedy the problem pointed out in (ii), Figure 2 plots the *preperihelion* normalized magnitudes  $H_{\Delta}$  as a function of heliocentric distance and fits the data by power laws, neglecting the minor dip showed in Figure 1

by C/2011 R1. Overall, the slopes are much steeper than  $r^{-2}$ , indicating that the comets were unquestionably active. However, with the exception of C/1948 E1, the steepness of the light curves near perihelion decreases with increasing intrinsic brightness. The pre-discovery observations of C/2011 R1 two years before perihelion (at distances of up to 7.5 AU from the Sun) are now plotted at the extreme right of the figure. The brightness of this comet at heliocentric distances below 4 AU varies as  $r^{-2.3}$ , a rate that jumps up rather abruptly to  $r^{-6}$  beyond 4 AU. A similar behavior is revealed by C/2018 C2, except that the numbers are very different: the comet's brightness varies as  $r^{-11}$  below 2.3 AU from the Sun, but as  $r^{-22}$  farther from the Sun. Interestingly, the total and nuclear CCD magnitudes reported for this comet were nearly identical, suggesting that it consisted of practically nothing but the nuclear condensation. Comet C/2006 L2 was not discovered early enough to exhibit the break in the slope, but the data show that the near-perihelion law  $r^{-3.7}$  applied to a distance of at least 2.8 AU. The extremely steep slope for C/1948 E1 is of course meaningless, merely fitting the brightness surge over a period of time during which the comet's heliocentric distance varied only very insignificantly.

It is noted that in contrast to Figure 1, 2I/Borisov is now in a region closer to the comets of average activ-

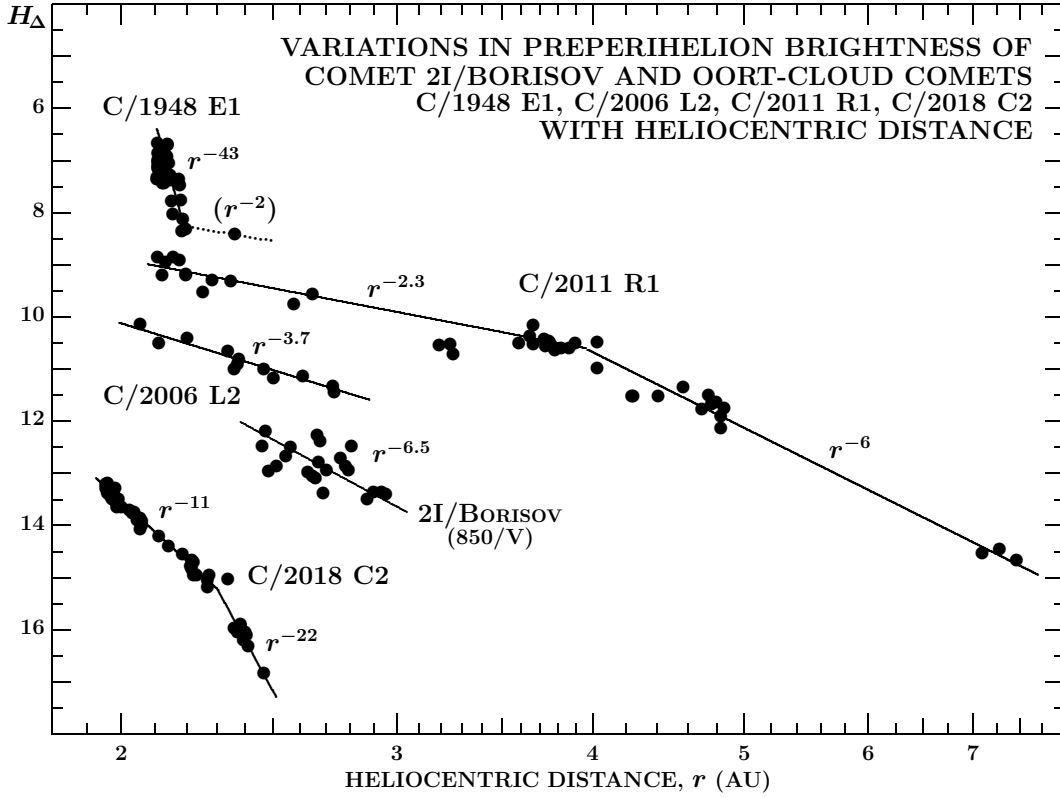


**Figure 2.** Plot of the preperihelion magnitudes from Figure 1 against heliocentric distance. It is noted that comet 2I/Borisov now moved up, away from C/2018 C2 and closer to C/2006 L2, an effect that is entirely due to the strongly hyperbolic orbital velocity of 2I. The pre-discovery observations of C/2011 R1 are incorporated at the extreme right of the plot. The curves that cover a wide enough interval of heliocentric distances consist of two parts, a steeper one farther from the Sun and a flatter one near perihelion. Comet C/1948 E1 is an exception because of a brightness surge it experienced shortly before perihelion. The future evolution of 2I/Borisov depends on the degree to which the corrected code 850 data are representative of this comet’s total-magnitude variations.

ity, its brightness varying, if the converted total visual magnitudes based on the code 850 *V* data are representative, as  $r^{-6.5}$ . If this fit refers to the pre-break (large- $r$ ) law and the break should occur in the coming days, near 2.4 AU from the Sun, followed by intrinsic variations fitting an  $r^{-2}$  rate, 2I should at perihelion be fainter than normalized magnitude 11 and appear then close to total visual magnitude 14, unless it undergoes an unexpected outburst. On the other hand, if the comet’s light curve has since discovery already been in the post-break segment, i.e., the break had occurred at a heliocentric distance larger than 3 AU, the comet should at perihelion be brighter than normalized magnitude 11 and become more luminous than total apparent visual magnitude 13 when at its brightest.

Over very short periods of time, on the order of one hour, the apparent brightness of 2I/Borisov is noticed to vary little, if at all, in some cases but rather dramatically, by more than 1 mag, in other cases. Such peculiar changes could be caused by the object’s rotation, but may also be an instrumental effect caused, for example, by inaccurate centering of a small scanning aperture on the condensation, especially in the presence of asymmetric features emanating from it. To determine the source of this inconsistency in photometric measurements, I present in Figure 3 individual overlapping magnitude data by nine different observers who imaged 2I over the same period of about 70 minutes on Septem-

ber 14. Four observers — codes 104, 470, C10, and C95 — noted no or minor variations with time, three observers — codes A77, J95, and Z80 — detected general fading, whereas two observers — codes 970 and B96 — reported distinct brightening. The verdict is thus obvious: the trend depends on the observer and is not a product of any physical changes of the comet.

## 6. DUST TAIL ORIENTATION AND PROJECTED LENGTH

To build up a dust tail takes time. The tail’s outlines are determined in part by the ejected grains’ velocities, which generally broaden the feature, but primarily by solar radiation pressure, which for each dust grain varies as its cross-sectional area and inversely as its mass. As a result, the magnitude of the effect varies inversely as the grain’s linear dimension. In addition, a grain’s position in the tail depends substantially on the time of its ejection. Solar radiation pressure does not force any grain out of the comet’s orbital plane but makes it move in a gravitational field that is weaker than the Sun’s gravitational field. The conservation-of-orbital-momentum law requires that the dust tail’s orientation be always constrained to a sector subtended by the prolonged radius vector  $\mathbf{RV}$  (antisolar direction) and the negative orbital-velocity vector  $-\mathbf{V}_{\text{orb}}$ . The deviation from the radius vector increases with the time elapsed since ejection, the dust released very long before perihelion trailing the nucleus in the orbit along the  $-\mathbf{V}_{\text{orb}}$  vector.

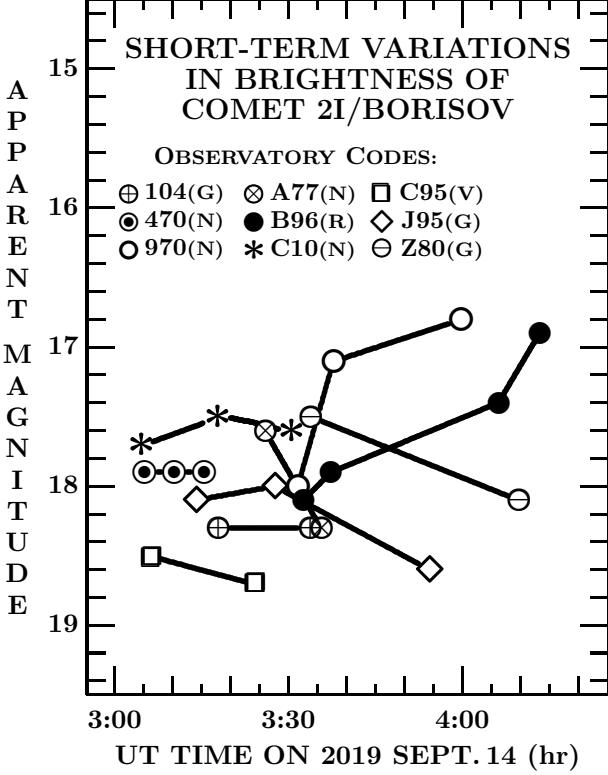


**Figure 3.** Short-term variations in the apparent brightness of 2I/Borisov, measured in images obtained at nine different observing sites, whose codes and magnitude types (measured with a variety of scanning apertures and in a variety of wavelength regions) are shown in the figure. In the course of the 70-minute period some sets show little or no variation with time, while other display a systematic increase or decrease, the evidence that the variations are an instrumental effect, not intrinsic to the comet.

When a tail is narrow and with no curvature, its direction is measured with high accuracy, so that comparison is possible with synchrotrons that unequivocally determine the times of dust grains' release from the nucleus. Just as the direction to a single dust grain's location from the nucleus, the orientation of the tail in projection onto the plane of the sky is defined by a position angle (reckoned from the north through east),  $PA_{\text{tail}}$ , that relative to the position angle of the radius vector,  $PA(\mathbf{RV})$ , and of the negative orbital-velocity vector,  $PA(-\mathbf{V}_{\text{orb}})$ , satisfies a condition

$$PA(-\mathbf{V}_{\text{orb}}) < PA_{\text{tail}} < PA(\mathbf{RV}), \quad (3)$$

when the Earth is located above the comet's orbital plane (i.e., the comet is seen from the Earth to orbit the Sun counterclockwise); or

$$PA(\mathbf{RV}) < PA_{\text{tail}} < PA(-\mathbf{V}_{\text{orb}}), \quad (4)$$

when the Earth is below the plane. It is assumed in these expressions that  $|PA(\mathbf{RV}) - PA(-\mathbf{V}_{\text{orb}})| < 180^\circ$ ; if this condition is not satisfied, it is necessary to restore it by adding  $360^\circ$  to the smaller of the two angles or by subtracting  $360^\circ$  from the larger one. At the time of the Earth's transit across the comet's orbital plane  $PA(-\mathbf{V}_{\text{orb}}) = PA(\mathbf{RV})$  or  $PA(-\mathbf{V}_{\text{orb}}) = PA(\mathbf{RV}) \pm 180^\circ$ , depending on the viewing geometry.

The issues addressed next are (i) the temporal evolution of dust content in the coma and tail of Oort Cloud comets with perihelia near 2 AU relative to those permanently beyond the snow line; and (ii) a modus operandi to find out where does 2I/Borisov fit into this scheme. I first compare images of 2I and two Oort Cloud analogs in Figure 4 and Table 2.<sup>6</sup> The choice of the two Oort Cloud comets reflects the need to examine both a span of activity and a range of orbital position. The displayed images of 2I, C/2014 AA<sub>52</sub>, and C/2011 R1 parallel the differences in the light curves. Even though no overall light curve is available for C/2014 AA<sub>52</sub>, the nuclear magnitude reported with the image (code W96) is 16.9 in an aperture of 16 600 km in diameter, which is equivalent to a normalized magnitude 14.7 after correcting for the geocentric distance and phase effect. A total CCD magnitude measured by code Q62 about 12 days apart (see footnote 3) was converted to the time of imaging observation to suggest the comet's normalized magnitude of 13.2, 1.5 mag brighter. With the standard correction to the total visual normalized magnitude, C/2014 AA<sub>52</sub> would be plotted in Figure 2 at 11.7 for  $r = 2.153$  AU, 3 mag brighter than the normalized nuclear magnitude. For C/2011 R1, the red nuclear magnitude reported with the image (code C10) is 15.7 in an aperture of 22 800 km in diameter, equivalent to a normalized nuclear magnitude of 13.1. This implies an expected magnitude of  $\sim 10$  in Figure 1 at  $t - t_\pi \simeq +170$  days, in perfect agreement with the fitted light curve. Finally, the magnitude reported with the image of 2I (code A77) is 16.8 in an aperture of 24 200 km in diameter, equivalent to a normalized nuclear magnitude of 14.1. One would expect the converted total visual magnitude of  $\sim 11$ , but the fit in Figure 2 shows the comet a little more than 1 mag fainter. 2I/Borisov looks much brighter than C/2014 AA<sub>52</sub> in Figure 4, due apparently to an instrumental effect ( $f/2.8$  vs  $f/8$ ).

The image of 2I in Figure 4 is reminiscent of a typical Oort Cloud comet at large heliocentric distance, even more so than the image of C/2011 R1, a comet with a more sizable nucleus and much more dust in the coma (Section 7). The position-angle range allowed for the tail by the condition (3) or (4) spans  $36^\circ$  for 2I,  $56^\circ$  for C/2014 AA<sub>52</sub>, and  $95^\circ$  for C/2011 R1. For all three comets the tail orientation fits the allowed range and Table 2 shows that in each case the tail's position angle, measured by the author from the images, is closer to the projected  $-\mathbf{V}_{\text{orb}}$  vector than the  $\mathbf{RV}$  vector. Comparison with radiation pressure computations suggests that dust grains in the tails of 2I and C/2014 AA<sub>52</sub>, both observed about two months before perihelion, were ejected from the nucleus some 200 days before perihelion, so that the tails were a little less than five months old when imaged. Because of the much higher orbital velocity of 2I, however, the heliocentric distance of this object at ejection was nearly 5 AU, while C/2014 AA<sub>52</sub> was only a little over 3 AU from the Sun when dust in its tail was released. The dust in the tail in the post-perihelion image of C/2011 R1 was ejected only about 50 days before perihelion, at a heliocentric distance of 2.2 AU; the tail thus was more than seven months old.

<sup>6</sup> The images were selected from the database available at the French website <http://lesia.obspm.fr/comets/index.php>.

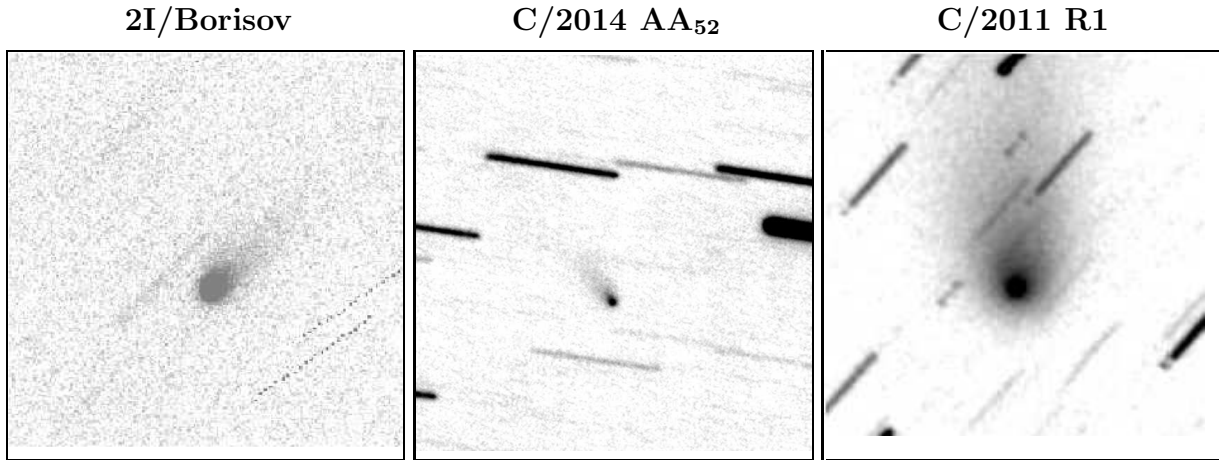


**Figure 4.** Comparison of the appearance of comets 2I/Borisov, C/2014 AA<sub>52</sub> (Catalina), and C/2011 R1 (McNaught). The image of 2I was taken by C. Rinner and F. Kugel on 2019 October 8.17 UT with a 40-cm f/2.8 reflector + CCD of the Observatoire Chante-Perdrix, Dauban, France (code A77); the image of C/2014 AA<sub>52</sub> by A. Maury and J.-F. Soulier on 2014 December 24.19 UT with a 40-cm f/8 Ritchey-Chrétien reflector + CCD of the Campo Catino Austral Observatory, San Pedro de Atacama, Chile (code W96); and the image of C/2011 R1 by J.-F. Soulier on 2013 April 7.06 UT with a 30-cm f/3 Newtonian reflector + CCD of the Observatoire Maisoncelles, Saint-Martin-du-Boschet, France (code C10). The common linear scale of the images is 330 000 km on a side. The north is up, east to the left for 2I and C/2014 AA<sub>52</sub>, but the south is up and east to the right for C/2011 R1. (Image credits: F. Kugel for 2I; J.-F. Soulier for C/2014 AA<sub>52</sub> and C/2011 R1.)

Insight into the physical processes involved is provided by another image of C/2011 R1, obtained by C. Rinner at Dauban on 2012 May 16.95 UT, 156 days before perihelion and about 100 days before the formation of the tail seen in the image taken on 2013 April 7. The 2012 image shows a tail extending at an estimated position angle of  $310^\circ$  and released around 170 days before Rinner’s observation. This suggests that the tail is being replenished as the comet orbits the Sun, but only by millimeter-sized and larger grains that show up in the tail only after having been subjected to radiation pressure over some period of time. This tail should project at a position angle of  $173^\circ$  in the 2013 image, but is missing. The obvious conclusion is that the grains disintegrated between the two observations, that is, in the general proximity of perihelion, which took place in October 2012.

The implied scenario is strongly reminiscent of comet C/1980 E1 (old designation 1980 I = 1980b; Bowell), an object with a perihelion distance of 3.36 AU. I noted that as the comet was approaching 5 AU on its way to perihelion, it appeared to display no obvious signs of contemporaneous activity but clear evidence of powerful emission, deep in the past, of millimeter-sized and larger dust grains expanding at extremely low, submeter-per-second, velocities (Sekanina 1982); the heliocentric distance of the dust emission was estimated at approximately 12 AU. Subsequently, A’Hearn et al. (1984) reported observations of the OH emission, first detected at about 5 AU, peaking between 4.5 and 5 AU preperihelion, and then subsiding, but with brief major outbursts overlapping. Linking their work to my finding, A’Hearn et al. interpreted OH as a product of the sublimation of water from the pre-existing halo of grains. They also remarked that, by contrast, CN appeared only when the comet was near perihelion.

Returning now to C/2011 R1, the tail that disappeared and was replaced with a more recent one, is likely to in-

dicate a process experienced by C/1980 E1, except for taking place at temperatures about 40 K higher. If activity of 2I follows the pattern of Oort Cloud comets, it too should undergo such changes, although perhaps on a smaller scale than C/2011 R1. An important, consistent property of all three comets in Table 2 is the absence of microscopic dust. In this sense, the behavior of 2I and the Oort Cloud analogs is alike.

Next is the issue of dust grain dimensions in the tail. Since the smaller the grain is the higher radiation pressure acceleration it is subjected to, the projected length of the tail provides, in the synchronic model, information on grains whose dimensions are the minimum. Both Oort Cloud comets in Table 2 consistently suggest that the smallest grains in the tail are millimeter sized. Whether or not the lower limit for 2I is significant remains to be seen. Unlike the orientation of a tail, its projected length is a very inaccurate quantity that depends critically on observational conditions, instrumentation, exposure time, etc.

Data for a second test of the tail orientation and length have been provided by Beyer’s (1950) visual monitoring of comet C/1948 E1 over a period of many months, as already remarked on briefly in Section 4. Figure 5 exhibits his measurements of temporal variations in the position angle of the tail; they are compared with the position angles of the  $\mathbf{RV}$  and  $-\mathbf{V}_{\text{orb}}$  vectors as well as with those of a few synchrones. It is noted that only one out of the more than 50 observations marginally defies the condition of the tail’s confinement to the sector subtended by the two vectors. This remarkable agreement is as much a testimonial to the exceptionally high quality of Beyer’s observational work as it is a confirmation that the model of dust tails works.<sup>7</sup>

<sup>7</sup> The measurements that Beyer marked as being uncertain have not been plotted.



**Table 2**  
Comparison of 2I/Borisov with C/2018 C2 before perihelion and C/2011 R1 after perihelion

|   | 2I/Borisov                             | C/2014 AA <sub>52</sub>                                   | C/2011 R1   |
|---|--|---|---|
| Time of observation (UT)                    | 2019 Oct 8.17                          | 2014 Dec 24.19  | 2013 Apr 7.06   |
| Time from perihelion <sup>a</sup> (days)    | −61.38                                 | −65.46  | +169.44   |
| Heliocentric distance (AU)                  | 2.424                                  | 2.153   | 2.857   |
| Geocentric distance (AU)                    | 2.873                                  | 2.084   | 1.961   |
| Phase angle                                 | 19°.5                                  | 26°.8   | 3°.5  |
| Cometocentric latitude of Earth             | −12°.8                                 | −22°.8  | +10°.8  |
| Position angle:                             |  |   |   |
| Prolonged radius vector                     | 293°.3                                 | 6°.0  | 260°.3  |
| Negative orbital velocity vector            | 329°.7                                 | 62°.2   | 165°.0  |
| Axis of tail                                | 318°                                   | 39°   | 181°  |
| Projected length of tail                    | 1'.1                                   | 0'.8  | 2'.6 <sup>b</sup>                                     |
| Model:                                      |  |   |   |
| Time of dust ejection <sup>a,c</sup> (days) | −200                                   | −200  | −50   |
| Heliocentric distance at ejection (AU)      | 4.8                                    | 3.1   | 2.2   |
| Minimum grain diameter <sup>d</sup> (mm)    | 0.35                                   | 1.3   | 1.9   |
| Observation:                                |  |   |   |
| Observer(s)                                 | C. Rinner, F. Kugel                    | A. Maury, J.-F. Soulier                                   | J.-F. Soulier   |
| Observing location                          | Obs. Chante-Perdrix,<br>Dauban, France | Campo Catino Austral Obs.,<br>San Pedro de Atacama, Chile | Obs. Maisoncelles,<br>Saint-Martin-du-Boschet, France |
| Observatory code                            | A77                                    | W96   | C10   |
| Telescope used                              | 40-cm f/2.8 reflector                  | 40-cm f/8 Ritchey-Chrétien                                | 30-cm f/3 Newtonian                                   |
| Filter                                      | none                                   | none  | red (Rc)  |
| Exposure time (min)                         | 33                                     | 30  | 30  |

**Notes.**

<sup>a</sup> Minus sign means before perihelion, plus sign after perihelion.

<sup>b</sup> Measured from an uncropped image.

<sup>c</sup> Reckoned from perihelion.

<sup>d</sup> At a unit scattering efficiency for radiation pressure and an assumed bulk grain density of  $0.5 \text{ g cm}^{-3}$ ; grain diameter varies as the first quantity and inversely as the second.

The diagnostic part of Figure 5 is the post-perihelion period of time when the difference between the position angles of the vectors  $\mathbf{RV}$  and  $-\mathbf{V}$  increases toward the maximum of  $180^\circ$  at the time of the Earth’s transit across the comet’s orbital plane, several weeks after Beyer’s measurements of the tail terminated.

In the period of time between 50 and 150 days after perihelion the tail’s position angle stays close to the position angle of the negative orbital velocity vector and varies in a manner that parallels the variations in the latter, but is entirely dissociated from the prolonged radius vector. The synchroes plotted in Figure 5 suggest that the observed tail consisted primarily of dust ejected between 300 and 100 days before perihelion. Beyer (1950) stated that the tail was slender, which suggests that no dust related to the post-perihelion activity was detected by his tail observations.

Figure 6 shows a plot of Beyer’s (1950) measurements of the projected length of the tail of C/1948 E1. Considerable scatter is now obvious, unquestionably because of variable seeing and the comet’s gradual fading. It turns out that around 130 days after perihelion Beyer could see only the part of the tail containing grains exceeding 1 mm in diameter, six times as large as those he observed when the comet was near perihelion.

Given the in-depth description of the complex evolution of the dust tails of Oort Cloud comets with perihelia near 2 AU and in view of the early signs that the tail of

2I/Borisov has been developing in a similar manner, I consider it useful to provide an extensive tail ephemeris for the interstellar object to assist in the forthcoming investigations of this type. Presented in Table 3, the individual columns list the ephemeris date (at a 20-day step), the solar elongation, the position vectors of the radius vector and negative orbital-velocity vector, the cometocentric latitude of the Earth, and, for each of three ejection times — 500 and 200 days before perihelion and at perihelion — the predicted position angle of the tail axis and the “extent,” which is the projected length of the tail defined by the location of dust grains subjected to a radiation pressure acceleration of 0.001 the Sun’s gravitational acceleration; if the scattering efficiency for radiation pressure of such grains is unity and their bulk density  $0.5 \text{ g cm}^{-3}$ , they are 2.3 mm in diameter, the smallest in the tail. For a given radiation pressure acceleration the grain size varies as the scattering efficiency and inversely as the bulk density. From the position angle of the tail measured in an image, the ejection time is determined by interpolating the tabulated position angles, then from the tail’s measured projected length the maximum radiation pressure acceleration is determined as 0.001 times the ratio of the projected length (in minutes of arc) to the interpolated value of the tabulated extent. For a given scattering efficiency and bulk density, the minimum diameter of grains in the tail varies inversely as the radiation pressure acceleration.

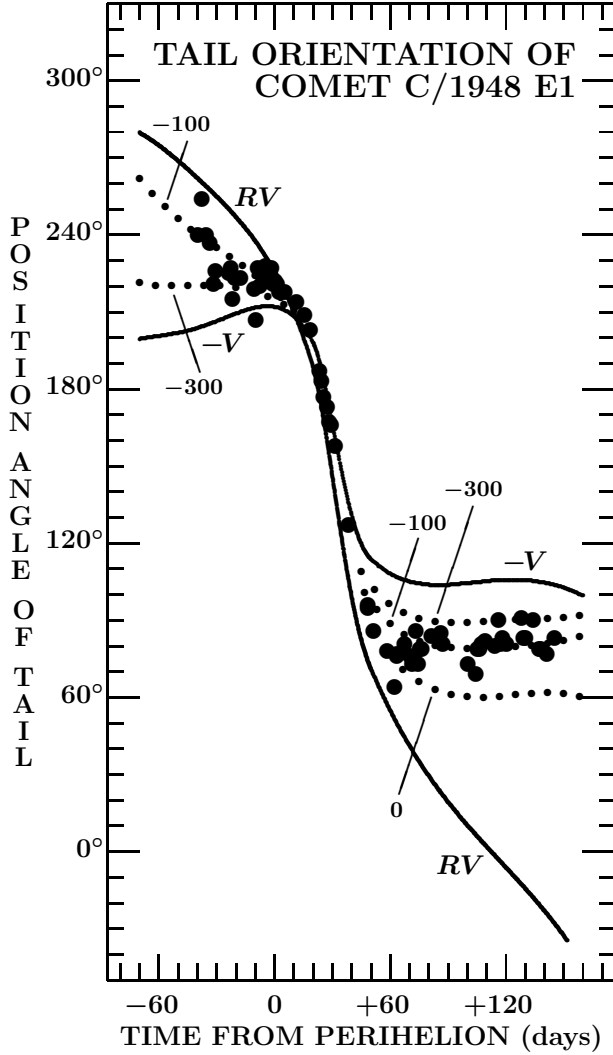


**Figure 5.** Plot of Beyer's (1950) measurements of the position angle of the tail axis of C/1948 E1 as a function of time reckoned from perihelion. The curves of temporal variations in the radius vector and the negative orbital-velocity vector are marked by  $RV$  and  $-V_{orb}$ , respectively. The dotted curves are position angles for ejection times 300 and 100 days before perihelion and at perihelion (0). Note that the observations made more than 50 days after perihelion indicate the tail was consistently oriented much closer to the direction of the  $-V_{orb}$  vector than the  $RV$  vector, confirming the absence of new emissions of microscopic dust. The comet passed through perihelion on 1948 May 16.61 TT.

#### 7. DUST PRODUCTION ALONG THE PREPERIHELION LEG OF THE ORBIT

In order to compare the amount of dust in the coma of a comet from non-uniform measurements, A'Hearn et al. (1984) introduced a product of an albedo, filling factor of dust in an aperture, and the aperture's size,  $Afp$ , a parameter that can easily be measured. Both A'Hearn et al. and Fink & Rubin (2012), who investigated the physical meaning of the parameter in considerable detail, focused on the  $Afp$  parameter as a proxy of the dust production rate. This implied relationship is justified on the grounds that the filling factor  $f$  depends on the number of dust grains in the column within the aperture, which in turn is proportional to the ratio of the dust production rate and dust expansion velocity. Fink & Rubin concluded

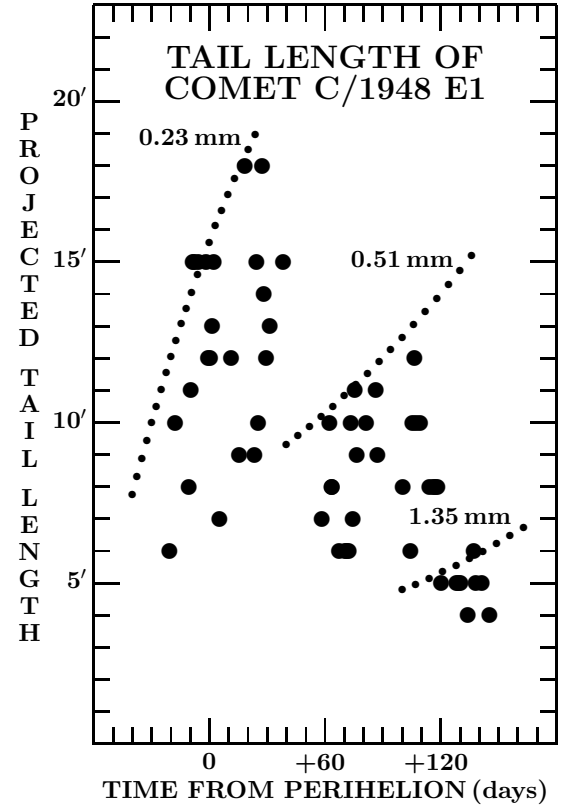


**Figure 6.** Plot of Beyer's (1950) measurements of the projected length of the tail of C/1948 E1 as a function of time reckoned from perihelion. The dotted curves are the temporal variations in the projected distance from the nucleus of dust grains ejected 200 days before perihelion and subjected to solar radiation pressure accelerations of, respectively, 0.010 (the steepest curve), 0.0045, and 0.0017 (the least steep curve) the Sun's gravitational acceleration; at a unit scattering efficiency for radiation pressure and an assumed bulk grain density of  $0.5 \text{ g cm}^{-3}$  the smallest grains detected by Beyer around perihelion, near 80 days after perihelion, and close to 130 days after perihelion are, respectively, 0.23 mm, 0.51 mm, and 1.35 mm in diameter, marking the dotted curves.

that submicron-sized grains, whose velocities are in the subkilometer-per-second range, contribute a large fraction to  $Afp$ . With these velocities, grains should evacuate the circumnuclear volume of space several tens of thousands kilometers in radius in a matter of one day or less, so this scenario naturally requires that new ejecta replace the lost dust. As the dust production rate is expected to correlate with the light curve, it should vary *inversely* as a power of heliocentric distance (Section 5).

The evidence from Section 6 overwhelmingly indicates that the tails of the 2I's analogs arriving from the Oort Cloud contained old, millimeter-sized and larger grains moving — as the tails' narrow breadth implies — at very low velocities. Because the dust in the tail is near the lower end of the grain population's size spectrum (i.e., near the upper end of the range of radiation pressure accelerations), still larger grains moving at still lower velocities should occupy the coma probed by the  $Afp$  parameter, some perhaps even gravitationally bound to the nucleus (at least along an early part of the inbound leg of the orbit). Under these circumstances, the  $Afp$  parameter measures the coma's (surviving) dust content along with any potential recent dust production rate.

**Table 3**  
Ephemeris for the Dust Tail of Comet 2I/Borisov

| Assumed dust emission time |                          |                |                   |                        |                        |        |                        |        |                    |        |  |
|----------------------------|--------------------------|----------------|-------------------|------------------------|------------------------|--------|------------------------|--------|--------------------|--------|--|
| Date<br>2019/20<br>(0 TT)  | Solar<br>elon-<br>gation | Position angle |                   | Earth<br>lati-<br>tude | 500 days preperihelion |        | 200 days preperihelion |        | At perihelion      |        |  |
|                            |                          | <i>RV</i>      | $-V_{\text{orb}}$ |                        | PA <sub>tail</sub>     | Extent | PA <sub>tail</sub>     | Extent | PA <sub>tail</sub> | Extent |  |
| Oct 4                      | 52°                      | 294°0          | 329°3             | −12°0                  | 323°7                  | 0′59   | 318°3                  | 0′14   | .....              | .....  |  |
| 24                         | 60                       | 291.1          | 330.9             | −15.5                  | 324.4                  | 0.91   | 319.2                  | 0.28   | .....              | .....  |  |
| Nov 13                     | 68                       | 289.4          | 331.0             | −17.4                  | 324.0                  | 1.35   | 319.2                  | 0.50   | .....              | .....  |  |
| Dec 3                      | 75                       | 289.4          | 329.1             | −16.6                  | 321.8                  | 1.84   | 317.8                  | 0.82   | .....              | .....  |  |
| 23                         | 81                       | 291.8          | 323.9             | −12.4                  | 317.3                  | 2.25   | 314.3                  | 1.18   | 297°3              | <0′01  |  |
| Jan 12                     | 87                       | 297.4          | 314.9             | −5.9                   | 310.6                  | 2.49   | 309.2                  | 1.49   | 302.6              | 0.05   |  |
| Feb 1                      | 93                       | 306.4          | 302.8             | +1.0                   | 303.8                  | 2.62   | 304.0                  | 1.72   | 305.1              | 0.13   |  |
| 21                         | 100                      | 319.5          | 291.5             | +7.0                   | 299.2                  | 2.71   | 301.0                  | 1.90   | 307.7              | 0.22   |  |
| Mar 12                     | 107                      | 337.5          | 285.9             | +11.2                  | 299.0                  | 2.80   | 301.8                  | 2.05   | 312.3              | 0.31   |  |
| Apr 1                      | 115                      | 359.9          | 286.5             | +13.5                  | 302.2                  | 2.87   | 305.5                  | 2.16   | 318.3              | 0.38   |  |
| 21                         | 121                      | 24.2           | 289.9             | +13.7                  | 305.7                  | 2.89   | 309.0                  | 2.21   | 322.5              | 0.43   |  |
| May 11                     | 124                      | 48.2           | 292.7             | +12.2                  | 306.9                  | 2.85   | 309.7                  | 2.21   | 322.6              | 0.46   |  |
| 31                         | 123                      | 69.9           | 294.1             | +9.5                   | 305.3                  | 2.75   | 307.6                  | 2.17   | 318.3              | 0.46   |  |
| June 20                    | 118                      | 87.8           | 294.2             | +6.3                   | 301.9                  | 2.63   | 303.3                  | 2.09   | 310.8              | 0.46   |  |
| July 10                    | 109                      | 101.3          | 293.4             | +3.0                   | 297.3                  | 2.50   | 298.0                  | 2.02   | 301.6              | 0.47   |  |
| 30                         | 99                       | 111.3          | 291.9             | +0.2                   | 292.1                  | 2.36   | 292.2                  | 1.94   | 292.3              | 0.48   |  |
| Aug 19                     | 87                       | 119.1          | 289.9             | −2.2                   | 286.7                  | 2.25   | 286.2                  | 1.88   | 283.8              | 0.51   |  |
| Sept 8                     | 75                       | 126.1          | 287.5             | −3.8                   | 281.2                  | 2.15   | 280.4                  | 1.84   | 276.4              | 0.54   |  |
| 28                         | 63                       | 133.6          | 284.7             | −4.8                   | 275.8                  | 2.08   | 274.8                  | 1.81   | 270.1              | 0.58   |  |
| Oct 18                     | 51                       | 143.3          | 281.2             | −5.1                   | 270.5                  | 2.02   | 269.4                  | 1.78   | 264.7              | 0.61   |  |

With these arguments in mind, I inspected the  $Afp$  database at the website of the Spanish Comet Hunters,<sup>8</sup> in which all entries are provided for a normalized aperture radius of 10 000 km. For correlation with Figure 2, I was interested only in the *preperihelion* data. Fairly sizable sets exist for C/2006 L2 (23 data points), C/2011 R1 (10), C/2014 AA<sub>52</sub> (20), and C/2018 C2 (12). There are 12 data points available for 2I, spanning the period of September 9 through October 8.

I corrected the  $Afp$  data for the phase effect with the use of the Marcus (2007) law and then plotted them against heliocentric distance  $r$  in Figure 7. The particularly striking feature is the plot for C/2014 AA<sub>52</sub>, the only comet for which the data cover a very wide range of  $r$ : the  $Afp$  value *decreases* with decreasing heliocentric distance as  $r^{-1/2}$ ! Although the light curve of this comet is not well established, five measurements of the total CCD magnitude by a single observer (code Q62) suggest that between 2.2 AU and 4.9 AU the preperihelion intrinsic brightness varied as approximately  $r^{-3}$ , a rate about midway between C/2011 R1 and C/2006 L2. In any case, the preperihelion light curve and  $Afp$  are absolutely incompatible. For C/2006 L2 the range of heliocentric distances covered by the preperihelion measurements of  $Afp$  is shorter, yet wide enough to show essentially no change between 2.0 AU and 2.7 AU from the Sun. For 2I/Borisov the same result is suggested by the measurements between 2.4 AU and 2.9 AU from the Sun. The preperihelion intervals of  $r$  for C/2011 R1 and C/2018 C2 are too short to allow a conclusion on the trend. However, the post-perihelion  $Afp$  data available for C/2011 R1 are lower than the preperihelion ones and

dropping as an inverse 4.5 power of heliocentric distance. The overall trend of  $Afp$  is reminiscent of the variations observed in C/1980 E1 by A'Hearn et al. (1984), who

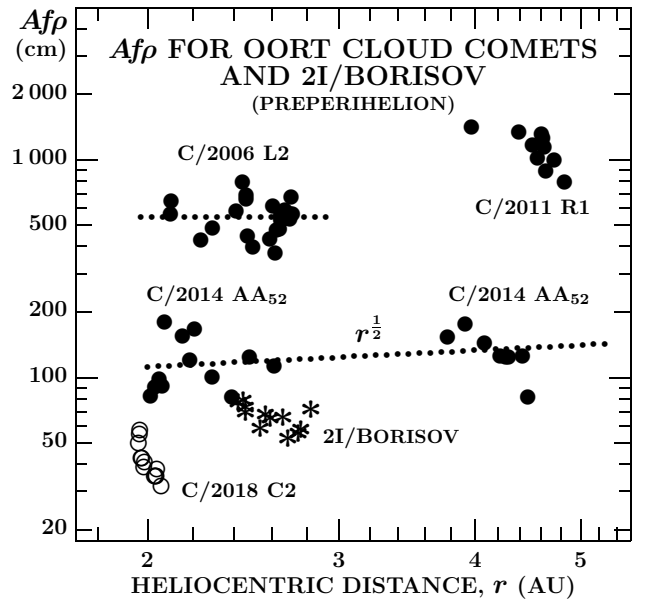


**Figure 7.** Plot of the dust production proxy parameter  $Afp$  as a function of heliocentric distance  $r$ . The data, normalized to a zero phase angle, are preperihelion measurements from a number of observatories reporting to the Spanish website of Comet Hunters, referring to four Oort Cloud comets — C/2006 L2, C/2011 R1, C/2014 AA<sub>52</sub>, C/2018 C2 — and to 2I/Borisov. The  $Afp$  parameter decreases with decreasing  $r$  for C/2014 AA<sub>52</sub> and stays essentially constant over a shorter interval of  $r$  for C/2006 L2. For C/2011 R1 and C/2018 C2 the range of  $r$  covered by the observations is too short to detect a trend; this is also true for 2I.

<sup>8</sup> See <http://astrosurf.com/cometas-obs>; the website is maintained by J. Castellano, E. Reina, and R. Naves.

determined that this parameter’s value dropped from 7000–8000 cm near 5 AU preperihelion to 3000–4000 cm near perihelion, thus following an  $\sim r^2$  law, much steeper than C/2014 AA<sub>52</sub> in Figure 7.

Among the Oort Cloud comets with perihelia near 2 AU,  $Afp$  appears to correlate with the light curve only in the sense that the brighter the comet is intrinsically at perihelion, the higher average value of  $Afp$  it has. Comet 2I/Borisov seems so far to fit this relationship — at least to the extent that one can find out from the limited database — on the fainter side; future observations should show whether this preliminary conclusion will continue to hold.

## 8. DISCUSSION AND CONCLUSIONS

In summary, the presented evidence strongly suggests that the pattern of activity of Oort Cloud comets with perihelia near 2 AU differs substantially from that of Oort Cloud comets whose perihelia exceed 4 AU. The difference stems from the position of the snow line in the Solar System — the more distant comets never experience the nucleus activity driven by the sublimation of water ice. On the other hand, both categories display effects of the absence of microscopic grains in the dust ejecta.

The snow line has ramifications for the evolution of the halo of large grains in the atmospheres of Oort Cloud comets. For example, the sublimation lifetime of an isothermal, pure icy grain of a bulk density of  $0.5 \text{ g cm}^{-3}$  and initially 1 mm in diameter amounts to more than 4 millennia at a heliocentric distance of 5 AU, 23 years at 4 AU, 85 days at 3.2 AU, 2 days at 2.5 AU, and about 8 hours at 2 AU. However, these numbers are only crude lower limits, because actual grains are not pure ice, but a mixture of refractory material and ice. If ice serves as a glue that holds the grains together, its gradual evacuation should progressively weaken the grains’ cohesion and result eventually — over much longer periods of time than are the above lifetimes — in their disintegration. And as this process is strongly heliocentric-distance dependent, the tail has an increasing tendency to disappear and the  $Afp$  value of the coma to drop steadily as the heliocentric distance continues to decrease below 4 AU. In addition, this process is accelerated by the fact that as the grains become less massive, the radiation pressure effects on them increase, thus speeding up their dispersion in space, away from the comet.

The absence of microscopic grains in the tails of Oort Cloud comets (their existence in the coma but not in the tail would require extremely short lifetimes) readily explains the instances of a missing dust tail near the radius vector. Sizable grains, subjected to radiation pressure accelerations not exceeding 1 percent of the Sun’s gravitational acceleration, reach the tail only after a prolonged time (if they survive), drifting in the meantime through the coma following their low-velocity release from the nucleus. By the time they get into the tail, their trajectories deviate notably from the direction of the radius vector.

As I concluded more than 40 years ago (Sekanina 1975), preperihelion activity of Oort Cloud comets is essentially continuous, with possible occasional surges, and those with perihelia below  $\sim 4$  AU undergo nucleus activity that is driven by the sublimation of water ice. Products of this activity overlap the surviving part of

the original halo of millimeter-sized and larger grains. This scenario is consistent with A’Hearn et al.’s (1984) extensive observations of C/1980 E1, whose perihelion distance was 3.36 AU, as well as with overwhelming evidence of “tail rejuvenation” among the comets with perihelia near 2 AU examined in this paper.

The complex evolution of Oort Cloud comets with perihelia at this distance from the Sun is illustrated by C/2011 R1. Its high preperihelion values of the  $Afp$  parameter imply the presence of a halo of early, nearly stationary dust grains in the atmosphere at heliocentric distances between 4 and 5 AU from the Sun. A preperihelion image shows a tail consisting of grains released at about 4 AU from the Sun, while the comet’s post-perihelion image in Figure 4 (and described in Table 2) documents the presence of dust grains whose ejection from the comet dates back to 2 months or so before perihelion. Thus, the products of the early activity failed to survive past perihelion. This finding is consistent with the evolution of another Oort Cloud comet, C/1950 K1 (Minkowski), of perihelion distance 2.57 AU, which I examined closely earlier (Sekanina 1975). The tail directions measured in some 40 images, taken over a period of nearly 300 days, showed that the observed dust ejecta were nearly always released from the comet between  $\sim 50$  and  $\sim 300$  days before observation and as late as the perihelion time. By contrast, Oort Cloud comets with perihelia near or beyond the snow line display evidence of early preperihelion activity at any subsequent time, including long after perihelion. For example, my detailed analysis of C/1954 O2 in an image taken by Osterbrock (1958) about 100 days after perihelion, when the comet was 3.96 AU from the Sun, shows that the outer extremity of the tail was populated by grains  $\sim 2$  mm in diameter released from the nucleus nearly three years before perihelion, at a heliocentric distance of 8.8 AU and that minor contributions to the tail may have been provided by grains ejected as late as 200 days before perihelion, 4.2 AU from the Sun, but not later (Sekanina 1975).

Accordingly, evidence shows that dust activity of most, if not all, Oort Cloud comets with perihelion distances under consideration drops rather rapidly, or possibly ceases for some, after perihelion; this does by no means prevent these comets from continuing to outgas. Among the objects examined in this paper, neither C/2011 R1 (Table 2) nor C/1948 E1 (Figure 5) show evidence for post-perihelion dust ejecta in their tails in images taken many months after perihelion. Also supporting this notion, though less conclusively, are (i) the systematic post-perihelion drop in the values of  $Afp$  of all comets in Table 1, for which the data are available; and (ii) the post-perihelion fading that is steeper than the preperihelion brightening seen in the light curves (Whipple 1978 and Figure 1).

Judging from the six weeks of data, the interstellar comet 2I/Borisov fits, in broad terms, the range of properties of Oort Cloud comets of the same perihelion distance as to its appearance, tail shape and orientation, and the dust production proxy parameter  $Afp$ . The available values of  $Afp$  suggest that the comet is a relatively small object, with probably a subkilometer-sized nucleus. Yet, the comet’s motion may be subjected, if at all, to only minor nongravitational effects. The detections of CN near 2.7 AU (Fitzsimmons et al. 2019a)

and C<sub>2</sub> at 2.5 AU from the Sun (Kareta et al. 2019; although questioned by Fitzsimmons et al. 2019b) also fit the general behavior of these Oort Cloud comets. The implied carbon chain depletion in 2I (regardless of whether C<sub>2</sub> was or was not detected) compares favorably with evidence on C/1999 S4 (Farnham et al. 2001), a probable Oort Cloud comet. Comet Borisov's activity appears to have already been driven by the sublimation of water ice in the past weeks; whether water is going to be detected is a matter of the emission rate and instrumental sensitivity. The comet's observations near and after perihelion will allow examination of a variety of diagnostic activity signatures to test the degree of 2I's similarity to Oort Cloud comets. The predicted tail ephemeris in Table 3 is intended to aid investigations of the evolution of dust production as the comet continues to pursue its motion along the strongly hyperbolic orbit.

This research was carried out at the Jet Propulsion Laboratory, California Institute of Technology, under contract with the National Aeronautics and Space Administration.

#### REFERENCES

- A'Hearn, M. F., Schleicher, D. G., Feldman, P. D., et al. 1984, *AJ*, 89, 579
- Bassot, J. A. L. 1907, *Astron. Nachr.*, 174, 127
- Beyer, M. 1950, *Astron. Nachr.*, 278, 217
- Bolin, B., Denneau, L., Wainscoat, R., et al. 2014, CBET 3812
- Dehnen, W., & Binney, J. J. 1998, *MNRAS*, 298, 387
- de León, J., Licandro, J., Serra-Ricart, M., et al. 2019, *Res. Notes AAS*, 3 (9), 131
- Dybczyński, P. A., Królikowska, M., & Wysoczańska, R. 2019, eprint arXiv:1909.10952
- Elenin, L. 2012, MPC 78724 and 78753
- Farnham, T. L., Schleicher, D. G., Woodney, L. M., et al. 2001, *Science*, 292, 1348
- Fink, U., & Rubin, M. 2012, *Icarus*, 221, 721
- Fitzsimmons, A., Hainaut, O., Yang, B., et al. 2019a, CBET 4670
- Fitzsimmons, A., Opitom, C., Hainaut, O., et al. 2019b, CBET 4679
- Gibbs, A. R., Grauer, A. D., Leonard, G. J., et al. 2018, MPC 109188 and 109209
- Green, D. W. E. 2019, CBET 4666
- Guzik, P., Drahus, M., Rusek, K., Waniak, W., et al. 2019, eprint arXiv:1909.05851
- Harrington, R. S. 1952, *PASP*, 64, 275
- Hill, R. E. 2008, *IAUC* 8945
- Hill, R. E., Gibbs, A. R., Kowalski, R. A., et al. 2012, MPC 78723 and 78753
- Jewitt, D., & Luu, J. 2019, eprint arXiv:1910.02547
- Kareta, T., Andrews, J., Noonan, J. W., et al. 2019, eprint arXiv:1910.03222
- Kowalski, R. A. 2014, CBET 3812
- Królikowska, M., & Dybczyński, P. A. 2013, *MNRAS*, 435, 440
- Królikowska, M., Sitarski, G., Pittich, E. M., et al. 2014, *A&A*, 571, A63
- Marcus, J. N. 2007, *Int. Comet Quart.*, 29, 39
- Marsden, B. G., Sekanina, Z., & Everhart, E. 1978, *AJ*, 83, 64
- McNaught, R. H. 2006, *IAUC* 8721
- McNaught, R. H. 2011a, *IAUC* 9213
- McNaught, R. H. 2011b, CBET 2810 and *IAUC* 9230
- McNaught, R. H. 2013, MPC 81939 and 81943
- Meech, K. J., Pittichová, J., Bar-Nun, A., et al. 2009, *Icarus*, 201, 719
- Merton, G. 1949, *MNRAS*, 109, 248
- Micheli, M. 2018, CBET 4501
- Mount Lemmon Survey 2018, CBET 4501
- O'Callaghan, J. 2019, *Sci. Amer.*, newsletter dated September 13
- Osterbrock, D. E. 1958, *ApJ*, 128, 95
- Porter, J. G. 1955, *MNRAS*, 115, 190
- Roemer, E. 1962, *PASP*, 74, 351
- Sekanina, Z. 1973, *Astrophys. Lett.*, 14, 175
- Sekanina, Z. 1975, *Icarus*, 25, 218
- Sekanina, Z. 1982, *AJ*, 87, 161
- Sekanina, Z. 2017, eprint arXiv:1712.03197
- Sekanina, Z. 2019a, eprint arXiv:1901.08704
- Sekanina, Z. 2019b, eprint arXiv:1903.06300
- Van Biesbroeck, G. 1950, *AJ*, 55, 53
- Weiss, E. 1907a, *Astron. Nachr.*, 176, 299
- Weiss, E. 1907b, *Astron. Nachr.*, 176, 327
- Whipple, F. L. 1978, *Moon & Plan.*, 18, 343
- Williams, G. V. 2014, MPEC 2014-D45
- Wolf, M. 1907, *Astron. Nachr.*, 176, 315
- Yang, B., Keane, J. V., Kelley, M. S. P., et al. 2019, CBET 4672